CHAPTER-3

INVESTIGATION OF NON-LINEAR FLUCTUATION DYNAMICS IN COMPLEX VISCOELASTIC ASTROFLUIDS

Abstract: *The non-linear evolutionary dynamics of self-gravitational instability of the model mentioned in Chapter-2 is semi-analytically investigated on the Jeansian scales of space and time.*[†] *A non-linear normal mode (local) analysis yields a Korteweg-de Vries (KdV) equation with a unique set of multi-parametric coefficients. The KdV dynamics excites an interesting spectral class of compressive solitary chain patterns as the evolutionary eigen-modes having atypical dynamical behaviour. Their diversified characteristic features are explained elaborately alongside phase-plane analysis. Various stabilizing (destabilizing) and accelerating (decelerating) factors of the instability are illustratively explored together with a validated reliability checkup. The relevancy of our investigated results in the context of super-dense compact astro-objects and their circumvent viscoelastic atmospheres is briefly outlined.*

3.1 INTRODUCTION

The dynamical mechanism responsible behind aggregation of matter and formation of various astrophysical structures, such as comets, asteroids, etc., in astro-cosmic environments are widely described by so-called gravitational (Jeans) instability [1]. Such instabilities occur when the internal pressure force (randomizing outward) is not sufficient to prevent the gravitational pressure (organizing inward) leading to dynamic fragmentation or collapse [2, 3].

A good number of investigations have been made on the gravitational instabilities in different self-gravitating fluid configurations in the past. The studies are mainly focused on exploring the various stabilizing and destabilizing agencies for the instability having a great impact in the initiation processes of astro-proto-structures [4-9]. In this direction, Chandrasekhar has found that the non-local self-gravitational collapse dynamics is independent of the action of both the uniform rotation and the uniform magnetic field separately or conjointly in an infinite homogenous fluidic medium [4]. Tsiklauri has investigated such instabilities in interstellar neutral gaseous cloud in the presence of weakly

[†]Kalita, D. and Karmakar, P. K. Nonlinear dynamics of gravitational instability in complex viscoelastic astrofluids. *AIP Advances*, 8: 085207. 1-15, 2018.

interacting massive particles (WIMPs). The WIMPs always reduce both the Jeans length and the Jeans mass for the onset of the instability in the cloud [7]. Besides, various instability features on gravitationally coupled complex bi-fluidic admixture of neutral fluid and dark matter fluid in the viscoelastic framework have also been reported in both the linear [5, 6] and non-linear [8] regimes. In addition, several authors have found that the linear instability in a self-gravitating viscoelastic medium occurs at a lower wavenumber against the purely neutral gas scenarios. The thermo-elastic pressure effects have been reported to introduce stabilizing influences to the instability [9, 10]. It can be eventually noted that the non-linear gravitational dynamics excitable in a self-gravitating complex viscoelastic medium in the presence of all the possible hydrodynamic complications has still been lying as an open problem to be well explored. In Chapter-2, we have discussed the linear gravitational instability excitable in neutral viscoelastic media under the simultaneous effects of polytropicity, fluid buoyancy, thermal fluctuation, volumetric expansion, and so forth [10]. The investigation of non-linear dynamics of such systems may alter the characteristics of various parameters in the system at a macroscopic level.

We, herein, propose a theoretical study on non-linear evolutionary dynamics of the gravitational instability of the model as described in Chapter-2. A non-linear normal mode (local) analysis around a hydrostatic homogeneous equilibrium yields a Korteweg-de Vries (KdV) equation with a unique set of multi-parametric coefficients. The analytic reliability of our calculations is reliably validated in the light of the existing reports in similar astrophysical environs. We construct a numerical illustrative standpoint to demonstrate how the KdV dynamics excites an interesting spectral class of compressive solitary chain patterns as the evolutionary eigen-modes of different features explained elaborately alongside applicability.

3.2 PHYSICAL MODEL AND FORMALISM

A generalized hydrodynamic (GH) model to study the non-linear evolution of the gravitational (Jeans) instability in a complex viscoelastic correlated fluid is considered. It takes into account all the possible realistic effects in the fluid dynamics, such as polytropicity, fluid buoyancy, thermal fluctuations, volumetric expansions, and so forth [10]. The viscoelasticity in the considered configuration arises due to the mutualistic interactions among the diversified constituents of the fluid [11]. As a result, it exhibits the properties of both viscosity and elasticity. The viscoelastic nature of the fluid is reported to cause the development of a plethora of collective excited waves, fluctuations and

oscillations [11, 12]. It subsequently indicates that astrophysical and cosmic fluids are to be categorically treated in a more profound justified fabric of the lowest-order viscoelasticity [12]. Such physical circumstances are realistically encountered in a large number of astro-cosmic environs, such as super-dense compact astro-objects and their surrounding gaseous atmospheres [9-14].

The macroscopic dynamics of the net flux-density (continuity equation) and the net force-density (momentum equation) of the fluid with all the customary notations [9, 10] are respectively given in a coupled form as

$$\frac{\partial \rho}{\partial t}+\frac{\partial}{\partial x}\left(\rho v\right)=0\ , \tag{3.1}$$

$$\left[1+\tau_m\left(\frac{\partial}{\partial t}+v\frac{\partial}{\partial x}\right)\right]\left[\rho\left(\frac{\partial}{\partial t}+v\frac{\partial}{\partial x}\right)v+\rho\left(1+\gamma T\right)\frac{\partial \psi}{\partial x}+\frac{c_s^2}{\Gamma}\frac{\partial \rho}{\partial x}\right]=\left[\varsigma+\frac{4}{3}\eta\right]\frac{\partial^2 v}{\partial x^2}\,, \tag{3.2}$$

where, ρ is the fluid material density, v is the bulk fluidic flow velocity, τ_m is the viscoelastic relaxation time, γ is the volumetric expansion coefficient, T is the fluid temperature, Γ is the polytropic exponent, and $n=1/\left(\Gamma-1\right)$ is the polytropic index [2, 3]. ψ is the non-local long-range gravitational potential. Furthermore, ς and η are the shear viscosity coefficient (first viscosity, offering resistance to flow) and bulk viscosity coefficient (second viscosity, offering resistance to volumetric expansion), respectively [5, 6, 8, 9]. The normal sound phase speed (Newtonian) in the fluid is given as $c_s=\left[\Gamma k_B T_0/m\right]^{1/2}$, with m as the constituent mass of the fluid and $k_B=1.38\times10^{-23}$ J K^{-1} as the Boltzmann heat-energy coupling constant [5, 6, 8].

The bulk fluidic state amid expansion and compression processes incorporating heat transfer is described by the polytropic equation of state given as

$$\left(\frac{\partial}{\partial t}+v\frac{\partial}{\partial x}\right)\left(P\rho^{-\Gamma}\right)=0, \tag{3.3}$$

where, $d/dt=\partial/\partial t+v\left(\partial/\partial x\right)$ is a linear temporal operator representing the convective (material) derivative. A few remarks on equation (3.3) are as the following. The gravitational instability in self-gravitating complex fluids naturalistically leads to aggregation or rarefaction of matter in space leading subsequently to structure formation. The interplay between gravitational force (inwards) and pressure force (outwards) generates various thermo-dynamical processes including compression and expansion of the constitutive fluid matter. These processes are explained in a combined generalized form

with the help of a polytropic equation of state $P\rho^{-\Gamma} = C$, where Γ is the polytropic exponent and C is the polytropic constant [2, 3]. The different values of Γ signify different polytropic processes depending on the involved thermodynamic. For instant, $\Gamma = 0$ for isobaric process, $\Gamma = 1$ for isothermal process, $\Gamma = \infty$ for isochoric process, $\Gamma = \gamma_a = c_p / c_v$ termed as the adiabatic exponent indicates to an adiabatic process, and so forth.

The evolution of the fluid temperature due to the microscopic thermal motion of the fluid constituent particles can be given with the help of heat diffusion law [10] as

$$\frac{\partial T}{\partial t} + v\frac{\partial T}{\partial x} = K_T \frac{\partial^2 T}{\partial x^2}, \tag{3.4}$$

where, K_T is the thermal diffusivity of the fluid. Similarly, the evolutionary equation for the the ρ - field [13] is cast as

$$\frac{\partial \rho}{\partial t} + v\frac{\partial \rho}{\partial x} = K_M \frac{\partial^2 \rho}{\partial x^2}, \tag{3.5}$$

where, K_M is mass diffusivity of the fluid. Finally, the closure is given by the gravitational Poisson equation [5, 6, 8, 9] which relates the spatial ψ -distribution with the ρ - field as

$$\frac{\partial^2 \psi}{\partial x^2} = 4\pi G(\rho - \rho_0), \tag{3.6}$$

where, $G = 6.67 \times 10^{-11}$ N m^2 kg^{-2} is the universal (Newtonian) gravitational constant via which the constituent particles of the fluid gravitationally interact. ρ_0 is the equilibrium density accounting for modelling the so-called Jeans swindle [1-3]. Needless to add that the swindle ignores the zeroth-order force field effects and considers the unperturbed macroscopic state of the fluid as a hydrostatic homogeneous one. This is possible when the inward self-gravitational attraction in the fluid is balanced by the outward expansive repulsion in the fluid caused by the cosmic pressure field force effects [1-3].

For a scale-invariant (scale-free, non-dimensional) analysis, a standard astrophysical normalization technique relevant on the Jeansian scales of space and time is used [5, 6, 8]. The normalized fluid governing equations (3.1)-(3.6), thus constructed, are respectively given as

$$\frac{\partial \rho^*}{\partial \tau} + \frac{\partial}{\partial \xi}\left(\rho^* M\right) = 0, \tag{3.7}$$

$$\left[1+\frac{\tau_m}{\tau_J}\left(\frac{\partial}{\partial\tau}+M\frac{\partial}{\partial\xi}\right)\right]\left[c_s\rho_0\rho^*\left(\frac{\partial}{\partial\tau}+M\frac{\partial}{\partial\xi}\right)M+c_s\rho_0\rho^*\left(1+\gamma T_0T^*\right)\frac{\partial\Psi}{\partial\xi}+\frac{c_s\rho_0}{\Gamma}\frac{\partial\rho^*}{\partial\xi}\right]$$

$$=\frac{1}{\lambda_J}\left(\varsigma+\frac{4}{3}\eta\right)\frac{\partial^2M}{\partial\xi^2}, \tag{3.8}$$

$$\left(\frac{\partial}{\partial\tau}+M\frac{\partial}{\partial\xi}\right)(P^*\rho^{*-\Gamma})=0, \tag{3.9}$$

$$\frac{\partial T^*}{\partial\tau}+M\frac{\partial T^*}{\partial\xi}=\left(\frac{K_T}{c_s\lambda_J}\right)\frac{\partial^2T^*}{\partial\xi^2}, \tag{3.10}$$

$$\frac{\partial\rho^*}{\partial\tau}+M\frac{\partial\rho^*}{\partial\xi}=\left(\frac{K_M}{c_s\lambda_J}\right)\frac{\partial^2\rho^*}{\partial\xi^2}, \tag{3.11}$$

$$\frac{\partial^2\Psi}{\partial\xi^2}=\rho^*-1. \tag{3.12}$$

Here, the independent parameters $\xi=x/\lambda_J$ and $\tau=t/\tau_J$ are the normalized distance and time, respectively. The symbols, $\lambda_J=c_s/\tau_J$ and $\tau_J=\omega_J^{-1}=\left(4\pi\rho_0G\right)^{-1/2}$, represent the Jeans scale length and Jeans time scale, respectively. $M=v/c_s$ is the normalized (by c_s) flow speed (Mach number) of the fluid. Ψ is the normalized (by c_s^2) gravitational potential. ρ^* is the normalized (by ρ_0) fluid material density. P^* is the normalized (by equilibrium pressure, P_0) pressure. T^* is the normalized (by equilibrium temperature, T_0) temperature.

We apply a standard reductive perturbation technique for investigating the non-linear instability dynamics in the considered self-gravitating complex fluid [15-18]. It is based on the assumption that the non-linearly perturbed relevant parameters are much feebler than their corresponding equilibrium parametric values. Accordingly, all the relevant dependent fluid parameters (F) undergo weakly non-linear perturbations (F_α) around their local hydrostatic homogeneous equilibrium parametric values (F_0) in an expansive form as follows

$$F=F_0+\sum_{\alpha=1}^{\infty}\varepsilon^\alpha F_\alpha, \tag{3.13}$$

$$F=[\rho^*\ \ M\ \ T^*\ \ P^*\ \ \Psi]^T, \tag{3.14}$$

$$F_0 = [1\ \ 0\ \ 1\ \ 1\ \ 0]^T, \tag{3.15}$$

$$F_\alpha = [\rho_\alpha^*\ \ M_\alpha\ \ T_\alpha^*\ \ P_\alpha^*\ \ \Psi_\alpha]^T, \tag{3.16}$$

The running spatiotemporal coordinates, ξ and τ, are now transformed into a new space defined by the stretched coordinates as $x^* := \varepsilon^{1/2}(\xi - \mu\tau)$ and $t^* := \varepsilon^{3/2}\tau$, respectively. Here, ε $(<<1)$ is a smallness order parameter that signifies the normalized relative wave amplitude of the lowest-order collective perturbations. In the newly defined space (x^*, t^*), the linear differential operators are auto-transformed as $\partial/\partial\xi \equiv \varepsilon^{1/2}(\partial/\partial x^*)$, $\partial^2/\partial\xi^2 \equiv \varepsilon(\partial^2/\partial x^{*2})$, and $\partial/\partial\tau \equiv \varepsilon^{3/2}(\partial/\partial t^*) - \mu\varepsilon^{1/2}(\partial/\partial x^*)$. Application of equations (3.13)-(3.16) in equations (3.7)-(3.12) generates different non-linearly perturbed forms of the relevant physical parameters. An order-by-order analysis on the both sides of equation (3.7) yields

$$O(\varepsilon^0): \frac{\partial M_1}{\partial x^*} - \mu\frac{\partial \rho_1^*}{\partial x^*} = 0, \tag{3.17}$$

$$O(\varepsilon^1): \frac{\partial \rho_1^*}{\partial t^*} - \mu\frac{\partial \rho_2^*}{\partial x^*} + \rho_1^*\frac{\partial M_1}{\partial x^*} + M_1\frac{\partial \rho_1^*}{\partial x^*} = 0, \text{ etc.} \tag{3.18}$$

Similarly, the perturbed form of equation (3.8) comes out as

$$O(\varepsilon^2): \mu\frac{\tau_m}{\tau_J}\left[\mu\frac{\partial^2 M_1}{\partial x^{*2}} - (1+\gamma T_0)\frac{\partial^2 \Psi_1}{\partial x^{*2}} - \frac{1}{\Gamma}\frac{\partial^2 \rho_1^*}{\partial x^{*2}}\right] - \frac{1}{\rho_0\lambda_J c_s}\left(\zeta + \frac{4}{3}\eta\right)\frac{\partial^2 M_1}{\partial x^{*2}} = 0, \text{etc.} \tag{3.19}$$

Again, the perturbed form of equation (3.9) reduces as

$$O(\varepsilon^1): \frac{\partial \rho_2^*}{\partial x^*} - \frac{\partial^3 \Psi_1^*}{\partial x^{*3}} = 0. \text{ etc.} \tag{3.20}$$

Now, equation (3.17) yields

$$M_1 = \mu\rho_1^*, \tag{3.21}$$

Again, from equation (3.18), one derives

$$\mu \frac{\partial \rho_2^*}{\partial x^*} = \frac{\partial \rho_1^*}{\partial t^*} + \rho_1^* \frac{\partial M_1}{\partial x^*} + M_1 \frac{\partial \rho_1^*}{\partial x^*} = 0, \tag{3.22}$$

$$\mu \frac{\partial \rho_2^*}{\partial x^*} = \frac{\partial \rho_1^*}{\partial t^*} + \rho_1^* \frac{\partial}{\partial x^*}\left(\mu \rho_1^*\right) + \mu \rho_1^* \frac{\partial \rho_1^*}{\partial x^*} = 0, \tag{3.23}$$

$$\frac{\partial \rho_2^*}{\partial x^*} = \frac{1}{\mu} \frac{\partial \rho_1^*}{\partial t^*} + 2\rho_1^* \frac{\partial \rho_1^*}{\partial x^*}. \tag{3.24}$$

Like-wise, from equation (3.19), we get

$$\mu \frac{\partial^2 M_1}{\partial x^{*2}} - \left(1+\gamma T_0\right) \frac{\partial^2 \Psi_1}{\partial x^{*2}} - \frac{1}{\Gamma} \frac{\partial^2 \rho_1^*}{\partial x^{*2}} = \frac{1}{\mu} \frac{\tau_J}{\tau_m} \frac{1}{\rho_0 \lambda_J c_s} \left(\zeta + \frac{4}{3}\eta\right) \frac{\partial^2 M_1}{\partial x^{*2}}, \tag{3.25}$$

$$\left(1+\gamma T_0\right) \frac{\partial^2 \Psi_1}{\partial x^{*2}} = \mu \frac{\partial^2}{\partial x^{*2}}\left(\mu \rho_1^*\right) - \frac{1}{\Gamma} \frac{\partial^2 \rho_1^*}{\partial x^{*2}} - \frac{1}{\mu} \frac{\tau_J}{\tau_m} \frac{1}{\rho_0 \lambda_J c_s} \left(\zeta + \frac{4}{3}\eta\right) \frac{\partial^2}{\partial x^{*2}}\left(\mu \rho_1^*\right), \tag{3.26}$$

$$\left(1+\gamma T_0\right) \frac{\partial^2 \Psi_1}{\partial x^{*2}} = \mu^2 \frac{\partial^2 \rho_1^*}{\partial x^{*2}} - \frac{1}{\Gamma} \frac{\partial^2 \rho_1^*}{\partial x^{*2}} - \frac{\tau_J}{\tau_m} \frac{1}{\rho_0 \lambda_J c_s} \left(\zeta + \frac{4}{3}\eta\right) \frac{\partial^2 \rho_1^*}{\partial x^{*2}}, \tag{3.27}$$

A spatial differentiation of equation (3.27) yields

$$\left(1+\gamma T_0\right) \frac{\partial^3 \Psi_1}{\partial x^{*3}} = \mu^2 \frac{\partial^3 \rho_1^*}{\partial x^{*3}} - \frac{1}{\Gamma} \frac{\partial^3 \rho_1^*}{\partial x^{*3}} - \frac{\tau_J}{\tau_m} \frac{1}{\rho_0 \lambda_J c_s} \left(\zeta + \frac{4}{3}\eta\right) \frac{\partial^3 \rho_1^*}{\partial x^{*3}}, \tag{3.28}$$

$$\frac{\partial^3 \Psi_1}{\partial x^{*3}} = \frac{1}{\left(1+\gamma T_0\right)} \left[\mu^2 \frac{\partial^3 \rho_1^*}{\partial x^{*3}} - \frac{1}{\Gamma} \frac{\partial^3 \rho_1^*}{\partial x^{*3}} - \frac{\tau_J}{\tau_m} \frac{1}{\rho_0 \lambda_J c_s} \left(\zeta + \frac{4}{3}\eta\right) \frac{\partial^3 \rho_1^*}{\partial x^{*3}} \right]. \tag{3.29}$$

Now, equation (3.20) in the light of equation (3.24) and equation (3.29) results in

$$\frac{1}{\left(1+\gamma T_0\right)} \left[\mu^2 - \frac{1}{\Gamma} - \frac{\tau_J}{\tau_m} \frac{1}{\rho_0 \lambda_J c_s} \left(\zeta + \frac{4}{3}\eta\right) \right] \frac{\partial^3 \rho_1^*}{\partial x^{*3}} - 2\rho_1^* \frac{\partial \rho_1^*}{\partial x^*} - \frac{1}{\mu} \frac{\partial \rho_1^*}{\partial t^*} = 0, \tag{3.30}$$

$$\frac{\partial \rho_1^*}{\partial t^*} + 2\mu \rho_1^* \frac{\partial \rho_1^*}{\partial x^*} - \frac{\mu}{\left(1+\gamma T_0\right)} \left[\mu^2 - \frac{1}{\Gamma} \left(1 + \frac{1}{\tau_m n_0 k_B T_0} \left(\zeta + \frac{4}{3}\eta \right) \right) \right] \frac{\partial^3 \rho_1^*}{\partial x^{*3}} = 0, \tag{3.31}$$

$$\frac{\partial \rho_1^*}{\partial t^*} + 2\mu \rho_1^* \frac{\partial \rho_1^*}{\partial x^*} + \frac{\mu}{\left(1+\gamma T_0\right)} \left[\frac{1}{\Gamma} \left(1 + \frac{\chi}{\tau_m n_0 k_B T_0} \right) - \mu^2 \right] \frac{\partial^3 \rho_1^*}{\partial x^{*3}} = 0, \tag{3.32}$$

$$\frac{\partial \rho_1^*}{\partial t^*} + A\rho_1^* \frac{\partial \rho_1^*}{\partial x^*} + B\frac{\partial^3 \rho_1^*}{\partial x^{*3}} = 0. \tag{3.33}$$

Here,

$$A = 2\mu, \tag{3.34}$$

$$B = \frac{\mu}{(1+\gamma T_0)}\left[\frac{1}{\Gamma}\left(1+\frac{\chi}{\tau_m n_0 k_B T_0}\right) - \mu^2\right]. \tag{3.35}$$

It is evident from equation (3.33) that the non-linear wave steepening (second term, convective effect due to fluidity) in our complex fluid model is caused by the referral frame velocity (via $A = 2\mu$, equation (3.34)). In contrast, the linear wave dispersion (third term, broadening effect) is sourced from the crisscross coupling of the conjoint influences caused by the referral frame velocity, volumetric expansion, thermo-polytropicity, and generalized effective viscosity (via *B*, equation (3.35)). We are interested in the steady-state (stationary) evolution of the fluctuations. It is done conveniently in a Galilean comoving coordinate transformation [15-18], $s = x^* - t^*$, such that linear differential operators go as $\partial/\partial x^* = \partial/\partial s$ and $\partial/\partial t^* = -\partial/\partial s$. So, equation (3.33) turns into an ordinary differential equation in a time-stationary form as

$$-\frac{\partial \rho_1^*}{\partial s} + A\rho_1^* \frac{\partial \rho_1^*}{\partial s} + B\frac{\partial^3 \rho_1^*}{\partial s^3} = 0. \tag{3.36}$$

It is seen that the weakly non-linear dynamics of the gravitational instability supported in the viscoelastic complex fluid is collectively governed by the stationary KdV equation (equation (3.36)). In order for exploring the macrophysical insights of the exact patterns of the instability, we execute a constructive numerical analysis to illustrate the results in the next section.

3.3 RESULTS AND DISCUSSIONS

The non-linear dynamics of the self-gravitational instability supported in a complex viscoelastic fluid model is analyzed in the GH framework on the Jeans scales of space and time. It includes the effects of polytropicity, thermal fluctuations, volumetric expansions, fluid buoyancy, and so forth. A non-linear normal mode analysis reduced the perturbed infinite planar fluid into a stationary KdV equation (equation (3.36)) governing the instability. The KdV equation is semi-analytically treated to explore various propagatory

features of the instability illustratively. The results are pictorially depicted as in figures 3.1-3.8.

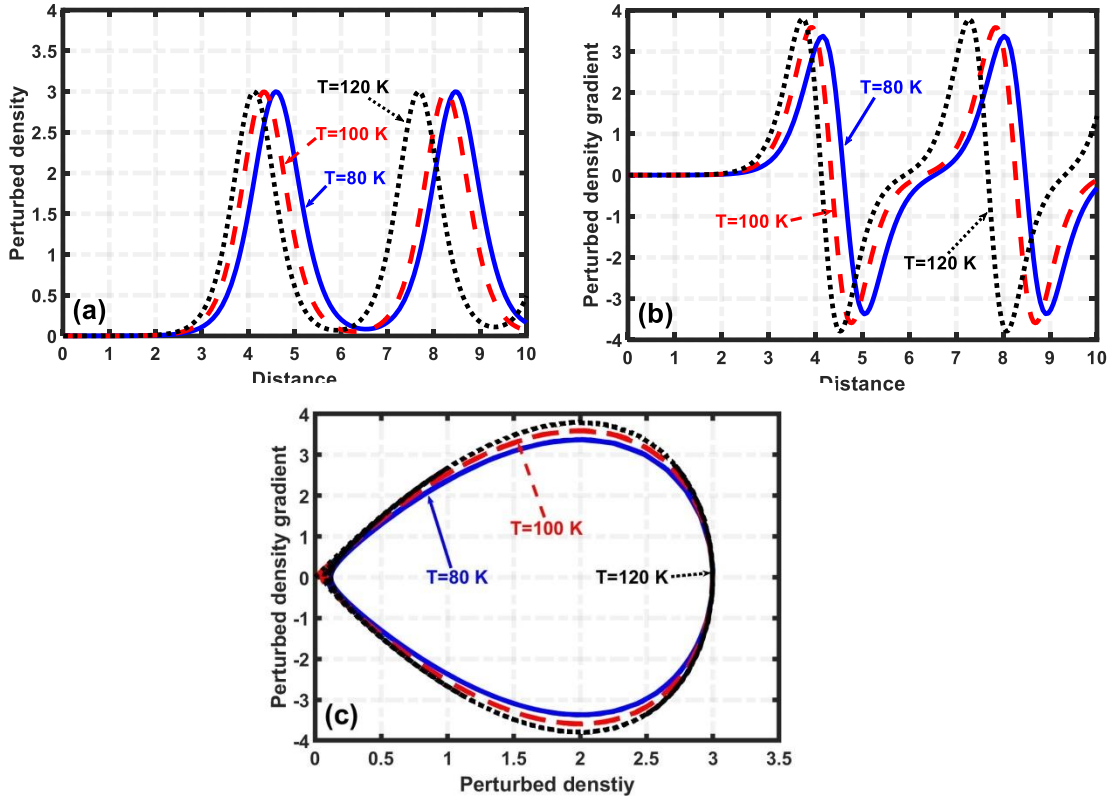

Figure 3.1: *Profile of the normalized (a) perturbed density with variation in the normalized distance, (b) perturbed density gradient with variation in the normalized distance, and (c) density phase portrait in a phase plane defined by the perturbed density and its gradient for different values of the equilibrium fluid temperature* (T_0).

In figure 3.1, we present the profile patterns of the normalized (a) perturbed density with variation in the normalized distance, (b) perturbed density gradient with variation in the normalized distance, and (c) density phase portrait in a phase plane defined by the perturbed density and its gradient for different equilibrium fluid temperature (T_0) values [19]. The different input values used in the numerical analysis are: polytropic index, $n=1$ [20], mean number density, $n_0 = 10^{22}\,\mathrm{m}^{-3}$ [21, 22], volumetric expansion coefficient, $\gamma = 10^{-2}$ K^{-1} [23], effective generalized viscosity, $\chi = 10^{-2}$ kg m^{-1} s^{-1} [14], viscoelastic relaxation time $\tau_m = 10^{-2}$ s [14], and normalized referral frame velocity $\mu = 0.5$ [16]. The various initial values used here are: $(\rho_1)_0 = 0.01$, $(d\rho_1/ds)_0 = 0.0001$ and

$\left(d^2\rho_1/ds^2\right)_0 = 0.00001$. It is seen that, for a given T_0 , the dynamics of the complex fluid evolves as a compressive solitary chain pattern. As T_0 increases, the maximum solitary peak shifts inwards with no change in the wave amplitude, thereby indicating that it travels faster towards the centre (figure 3.1(a)). As a consequence, the wave patterns reorganize the fluid against the perturbation in a new redistributed form in the form of the fluid material transportation. It is further seen that, as T_0 increases, the amplitude of the field fluctuations, evolving as an admixture of compressive and rarefactive solitary chains, enhances with the peak positions shifting inwards (figure 3.1(b)). It indicates that, the fluid becomes unstable with the T_0 -enhancement, and vice-versa. The phase portrait trajectories emerging out from the fixed point indicate stable limit cycles of the fluid dynamical oscillations. The closed nature of the geometrical patterns indeed reflects that the weakly non-linear fluid fluctuation dynamics is a conservative one. It is further revealed in the phase-plane analysis that, only the fixed points in all the non-chaotic phase portraits remain absolutely unaffected irrespective of the T_0 - enhancement (figure 3.1(c)). Alternatively speaking, the fluid density extrema are stable fixed points. Thus, T_0 acts as a destabilizing agent for the complex self-gravitating fluid instability with the help of bi-fold action as the solitary pulse-peak shifts towards the centre (figure 3.1(a)), and perturbed density fluid amplitude enhancer (figure 3.1(b)).

As in figure 3.2, we display the same as figure 3.1, but for different normalized referral frame velocity (μ) values at a fixed temperature, $T_0 = 80$ K. It is seen that, as the μ-value increases, the maximum solitary peak position shifts outwards with the wave amplitude getting reduced, and vice-versa (figure 3.2(a)). It indicates that the solitary peaks travel slower towards the centre. Also, the amplitude of the corresponding field fluctuations decreases with increase in μ, and vice-versa (figure 3.2(b)). It is further seen that an increment in the μ-value renders a phase curve contraction; but always in a closed conservative form with variable amplitude; and vice-versa (figure 3.2(c)). It may be physically attributable to the relative de-coherent (non-resonant) interaction between the gravitational fluid fluctuations of external macroscopic origin and the background acoustic random fluctuations of internal microscopic origin. In all and totality, it is found that the referral velocity, μ, acts as an amplitude reducer. Therefore, μ acts as a stabilizing agent to the fluid against the non-local self-gravitational collapse dynamics.

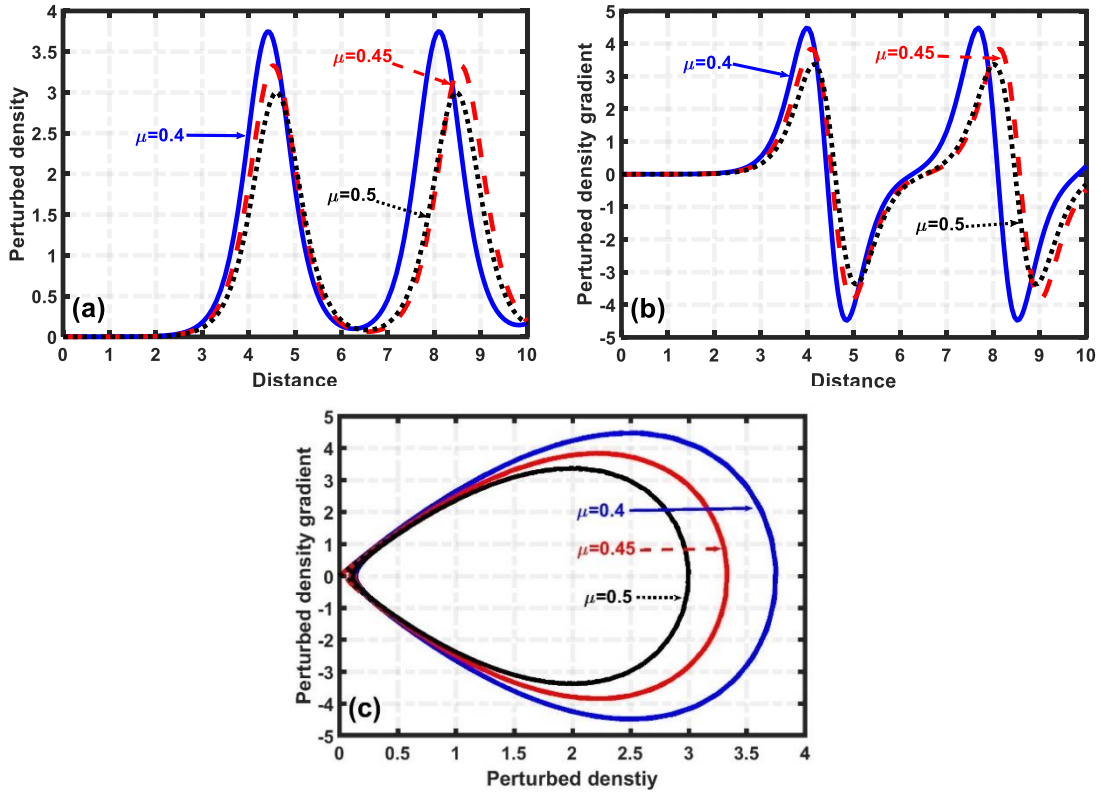

Figure 3.2: *Same as figure 3.1, but for different values of the normalized referral frame velocity* μ *at a fixed* $T_0 = 80\ K$.

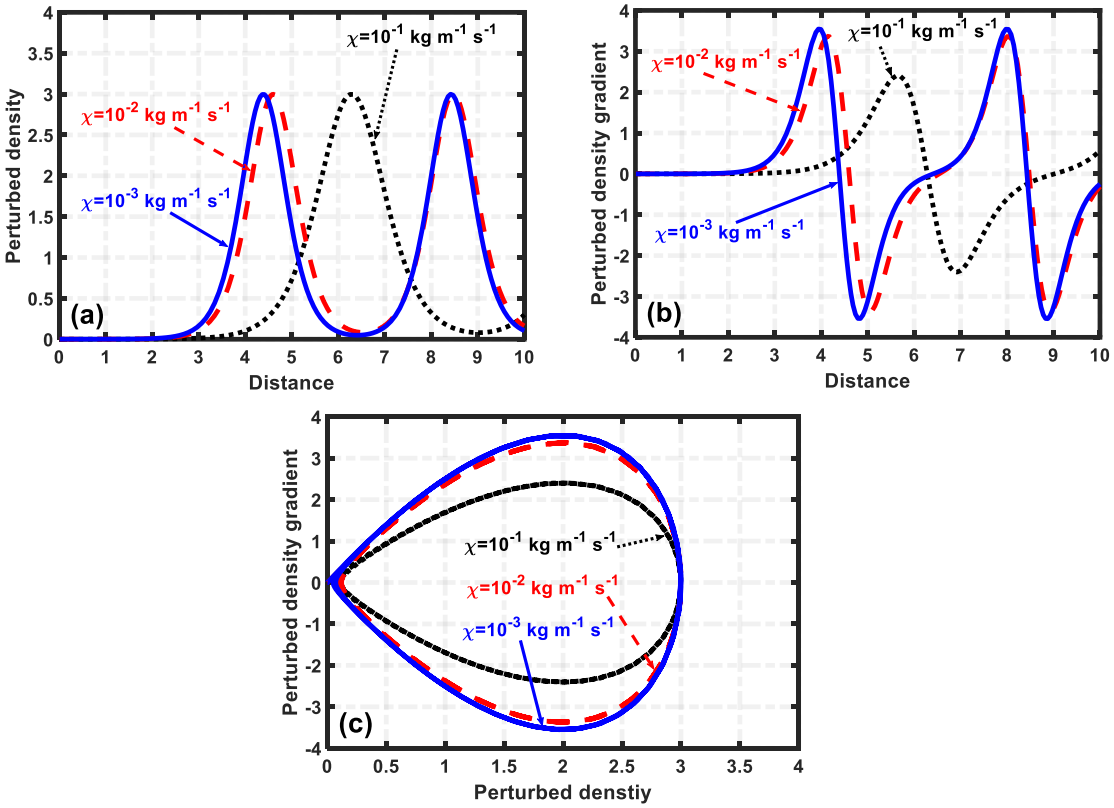

Figure 3.3: *Same as figure 3.1, but for different values of the generalized effective viscosity* χ *at a fixed temperature* $T_0 = 80\ K$.

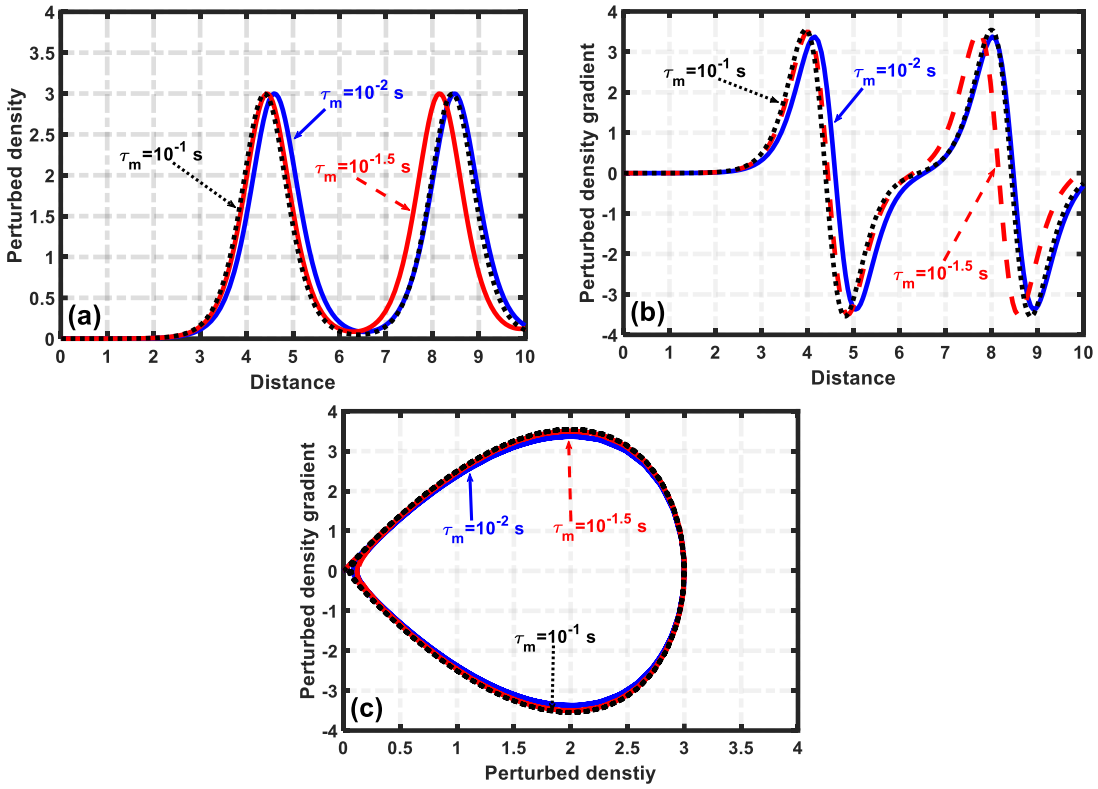

Figure 3.4: *Same as figure 3.1, but for different values of the viscoelastic relaxation time* τ_m *at a fixed temperature* $T_0 = 80$ *K.*

In figure 3.3, we show the same as figure 3.1, but for different generalized effective viscosity (χ) values with a fixed temperature, $T_0 = 80$ K. It is found that, as χ increases, solitary peak position shifts outward with no change in amplitude (figure 3.3(a)). It indicates that the solitary peaks travel slower towards the centre. The fluid viscosity is high enough to resist the bulk fluid flow and volumetric fluid expansion. So, the fluid is reorganized against the perturbation applied to it. In addition, the amplitude of the corresponding field fluctuations decreases with the χ-value, and vice-versa (figure 3.3(b)). Moreover, it is found that the phase curves are in closed conservative form, remaining unaffected with χ at the fixed point (figure 3.3(c)). As a consequence, χ acts as a stabilizing agent to the fluid instability dynamics.

In figure 3.4, we portray the similar periodic solitary chain patterns as figure 3.1, but now for different viscoelastic relaxation time (τ_m) values at a fixed temperature, $T_0 = 80$ K. The instability evolves here (figure 3.4) in a similar fashion as in figure 3.1, but

in new conditions. The only distinction found here is that, as τ_m increases, the amplitude of the solitary field fluctuations, evolving as an admixture of compressive and rarefactive solitary chains, enhances with the peak positions shifting inwards (figure 3.4(b)). Thus, τ_m acts as destabilizing agent to the instability dynamics.

In figure 3.5, we depict the same as figure 3.1, but for different mean equilibrium number density (n_0) values at a fixed temperature, $T_0 = 80$ K. It is found that the evolutionary instability patterns here are the same as in figure 3.1. As a result, we infer that n_0 acts as the destabilizing agent to the instability leading to diversified structure formation processes [5-9].

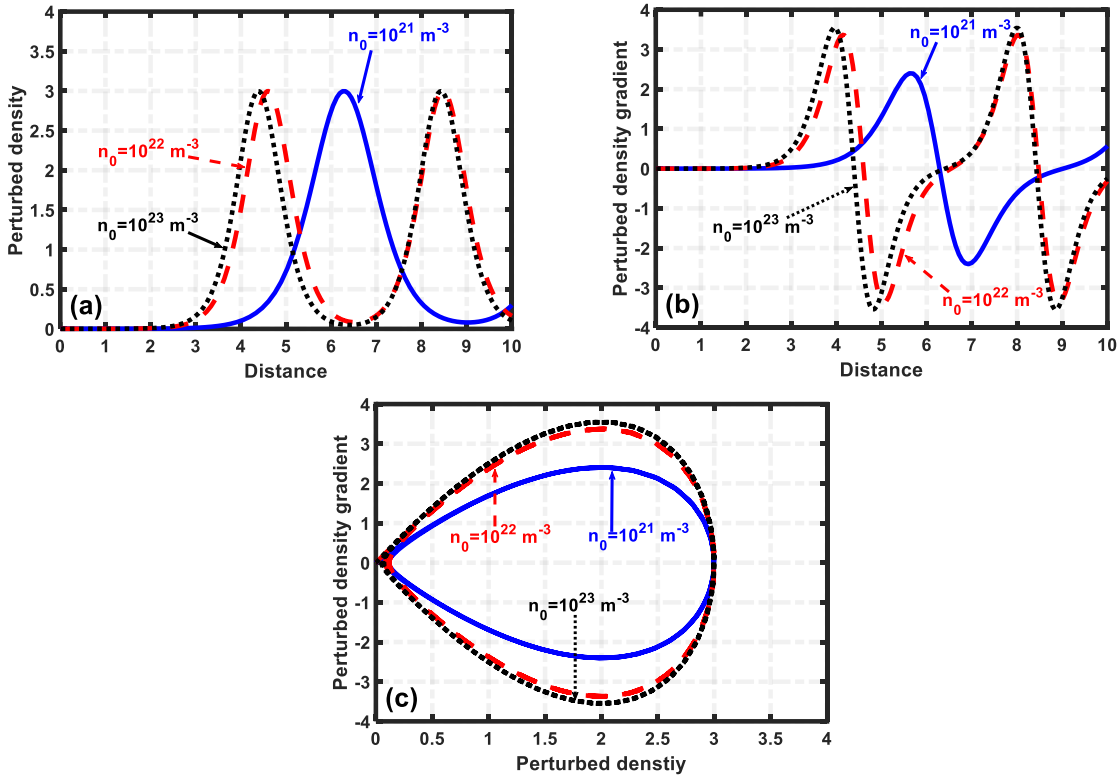

Figure 3.5: *Same as figure 3.1, but for different values of the mean equilibrium number density* n_0 *at a fixed temperature* $T_0 = 80$ *K.*

In figure 3.6, we display the same as figure 3.1, but for different polytropic index (n) values at a fixed temperature, $T_0 = 140$ K. The variation of the instability patterns due to the different n-values are the same as figure 3.3. So, it can be inferred that n acts as a stabilizing agent to the fluctuation dynamics leading to non-local structure formation mechanisms.

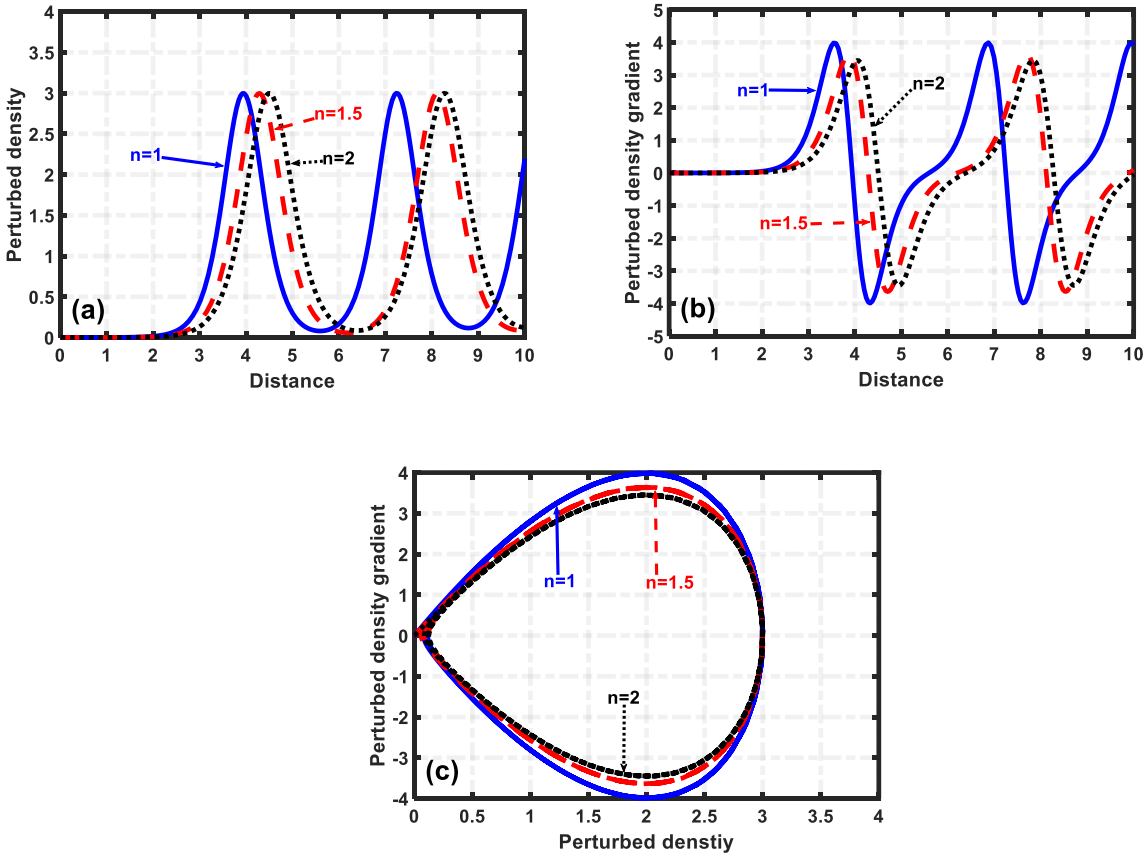

Figure 3.6: *Same as figure 3.1, but for different values of polytropic index* n *at a fixed temperature* $T_0 = 140$ *K.*

In figure 3.7, we portray the same as figure 3.1, but for different volumetric exponent (γ) values at a fixed temperature, $T_0 = 80$ K. It is seen that the peak-to-peak separation in the perturbed potential increases with decrease in the volumetric thermal expansion, and vice-versa. It is interesting to note that the potential fluctuation amplitude remains almost the same (figure 3.7(a)). The corresponding field fluctuation evolves in such a way that the peak-to-peak separation increases with decrease in the volumetric thermal expansion, but the field amplitude goes on reducing; and vice-versa (figure 3.7(b)). The remaining instability patterns, particularly in the geometrical trajectories (figure 3.7(c)) due to the γ-variation, is the same as figure 3.1. The main physical mechanism responsible behind may be ascribable to the fact that larger the fluid volume, more massive the fluid is; thereby, the fluid getting more unstable, and vice-versa. As an overall consequence, it can be concluded that volumetric exponent behaves as a destabilizing agency to the instability evolutionary dynamics.

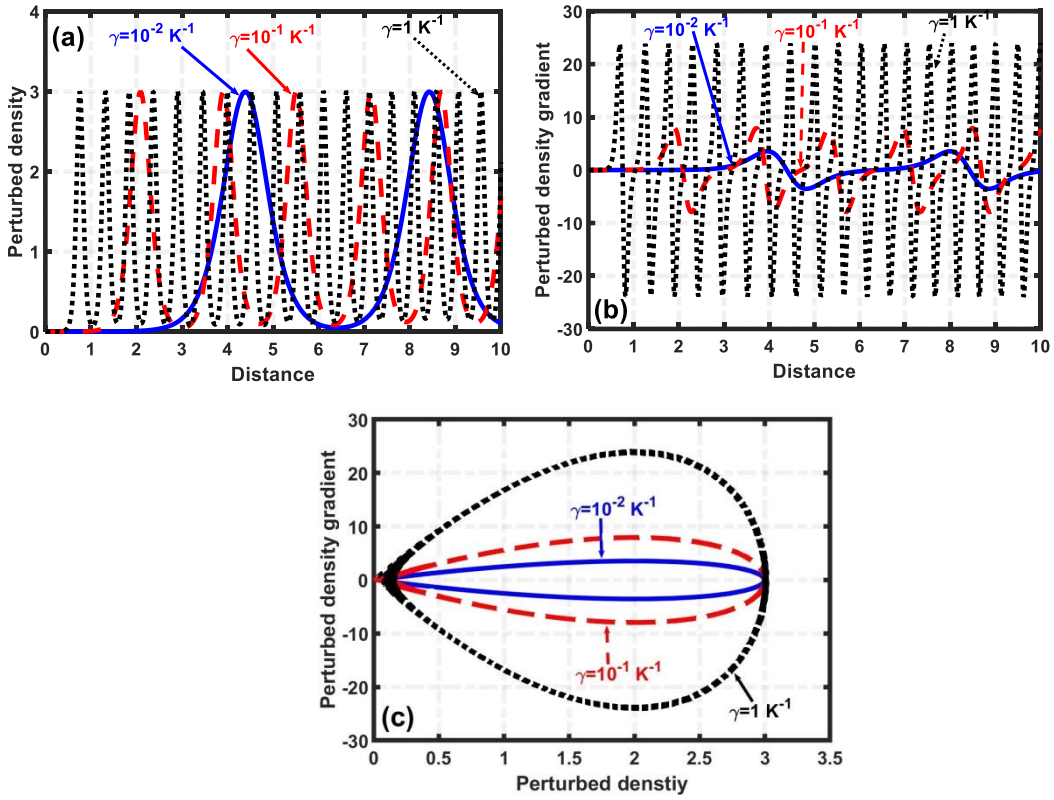

Figure 3.7: *Same as figure 3.1, but for different values of volumetric exponent* γ *at a fixed temperature* $T_0 = 80\ K$.

In figure 3.8, we show the same as figure 3.1, but for different fluid configurations on a comparative footing for a fixed $T_0 = 80$ K. The different lines link to (i) pure inviscid nebular fluid model (blue solid line), (ii) non-ideal viscoelastic fluid model (red dashed line), and (iii) our complex non-ideal viscoelastic fluid (black dotted line), respectively. In case (i), we take $n_0 = 10^{22}$ m^{-3}, and $\Gamma = \left(1 + n^{-1}\right) = 1$. In case (ii), we take $\chi = 10^{-1}$ kg m^{-1} s^{-1}, and $\tau_m = 10^{-2}$ s in addition to case (i). In case (iii), we take $n = 1$, and $\gamma = 10^{-2}$ K^{-1} in addition to case (ii). It is seen that the solitary peak-to-peak separation decreases with enhanced fluid complications, and vice-versa. Thus, the peak-to-peak separation in case (i) is the maximum and that in case (iii) is the minimum with case (ii) lying as an intermediate in the peak-separation value in the coordination space. It is clearly evident that viscoelastic non-ideal fluids are more stable than pure ideal inviscid fluids against non-local gravitational collapse due to the combined action stemming from the effects of temperature, generalized viscosity, relaxation time, referral frame velocity and number density. Our

considered complex fluid is more unstable than the remaining two fluids as mentioned above. This is due to the additional destabilizing effects by the thermometric volume expansion in contrast with those without thermal expansion.

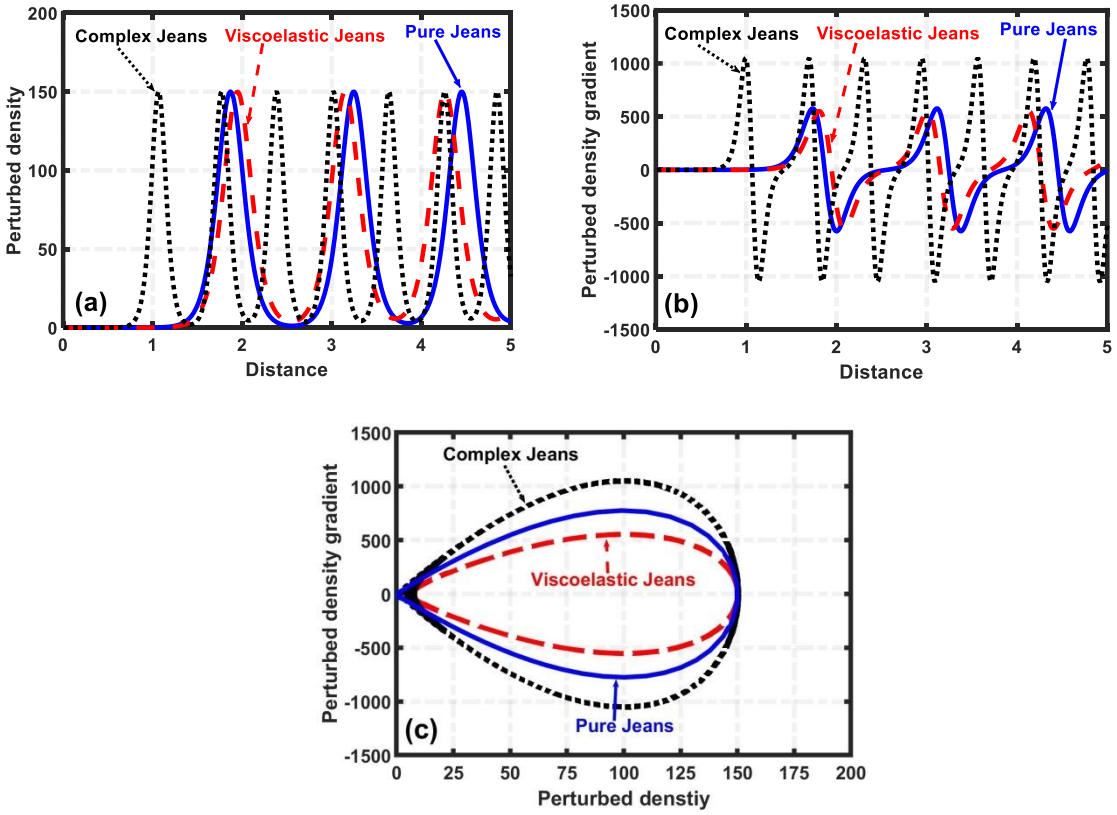

Figure 3.8: *Same as figure 3.1, but for different fluid configurations on a comparative footing for a fixed* $T_0 = 80\ K$.

It may be noted here that in the case of the Newtonian fluids, the threshold condition required for the onset of the linear gravitational instability is given on the angular wavenumber with all the generic notations as $k < k_J$, where $k_J = \sqrt{4\pi G\rho_0}\,/c_s$ is the critical Jeans angular wavenumber [9]. In the present case of the non-linear gravitational instability, the instability onset condition is analogously given by the fact that the scale size of the self-gravitating viscoelastic fluids must be greater than λ_J, which means that the normalized cloud fluid size must be greater than 1 for the gravitational perturbation to grow as clearly evident in figures (3.1)-(3.8), where $\lambda_J = k_J^{-1}$ is the critical Jeans wavelength.

In order for further validation of our results, it would be nice to compare the presented study, despite its infancy stage, with the existing closely related reports, if any. Accordingly, let us now compare the analysis at least with the gravitational fluctuation

dynamics associated with the co-rotating viscoelastic neutral gas fluid gravitationally coupled with the viscoelastic dark matter fluid [8]. In this case, the dynamics is conjointly governed by a unique conjugated pair of viscoelastic forced Burgers (VFB) equations thereby yielding solitons and shocks of hybrid characteristics. The non-linear eigen-mode patterns explored here are furthermore in good agreement with the non-linear waves excitable as "clump-filament entities" in self-gravitating star-forming molecular clouds with partial ionization previously reported elsewhere [24]. In addition, the investigated non-linear wave features may be used as an alternative analytic element to understand the various interesting multi-space satellite (e.g., Freja, Viking, and so forth) observations on the existence of diversified atypical non-linear solitary pulse-like wave disturbances in different broad-band astro-space-cosmic environs collectively [25-27]. The theoretically investigated non-linear density wave structures are fairly in good accord with the observations of the irregular pulse-pattern features. It hereby judiciously puts forward both the analytic reliability and astro-space applicability of the proposed semi-analytic fluid stability analysis alongside the associated non-linear wave structures. Most importantly, the investigated eigen-mode signatures could play influential concretized roles in the mechanism of energization, transportation and redistribution of the fluid constitutive particle producing non-homologous dense sites in diversified interstellar fluid media subsequently converted into bounded neonatal astrophysical structures, such as stellesimals, planetsimals, and so forth.

3.4 CONCLUSIONS

A semi-analytic investigation is systematically carried out to see the non-linear evolutionary dynamics of self-gravitating viscoelastic complex fluids on the Jeansian scales of space and time. The complex fluid is assumed to be illimitable in nature, thereby paving the wave for planar geometry approximation. It concurrently incorporates key realistic influential factors relevant for astrofluid, such as polytropicity, thermal fluctuations, volumetric expansions, fluid buoyancy, etc. A new basic set of governing generalized fluid equations is procedurally formulated in the light of all such key factors. A standard reductive perturbation technique reduces the non-linearly perturbed fluid into a KdV equation of atypical shape and construct.

A judicious numerical analysis is performed to explore various stabilizing and destabilizing factors to the fluid instability dynamics in an illustrative platform. The analysis shows that the perturbed density evolves as an admixture of compressive and

rarefactive solitary chain patterns. The closed loops in the form of geometrical trajectories confirm the conservative nature of the weakly non-linear perturbation dynamics in the fluid system. It is found that the fluid temperature, viscoelastic relaxation time, number density and volumetric expansion play as destabilizing agencies to the instability dynamics. In contrast, referral frame velocity, generalized effective viscosity and polytropic index act as a stabilizing agent to the fluctuating system against the non-local gravity. A comparative analysis is provided for a comparative reliability checkup of our model under the auspice of pure ideal nebular fluid, non-ideal viscoelastic fluid and our considered complex fluid simultaneously. It is furthermore found that the complex fluids are the least stable, viscoelastic fluids are the most stable, and pure ideal nebular fluid is in intermediate stability lying between the two. The characteristics of key instability featuring factors is shown in Table 3.1 in the Appendix-3.A.

The analytic reliability and astro-space applicability of the proposed semi-analytic fluid stability analysis alongside the associated non-linear wave structures resembling the various previously reported multi-space satellite observations are briefly indicated. The investigated eigen-mode signatures may be relevant in the mechanism of energization, transportation and redistribution of the fluid constitutive particle producing non-homologous dense sites in diversified interstellar fluid media subsequently converted into bounded neonatal astro-physical structures, such as stellesimals, planetsimals, etc. The eigen-mode structures may also be of extensive significance in understanding the complex fluid dynamics and associated instabilities in super-dense compact astroobjects, their surrounding atmospheres, and so forth.

REFERENCES

[1] Jeans, J. H. The stability of a spherical nebula. *Philosophical Transactions of the Royal Society*, 199: 1-53, 1902.

[2] Binney, J. and Tremaine, S. *Galactic Dynamics.* Princeton university press, Princeton, 1987.

[3] Mo, H., Van den Bosch, F., and White, S. *Galaxy Formation and Evolution.* Cambridge University Press, Cambridge, 2010.

[4] Chandrasekhar, S. *Hydrodynamic and Hydromagnetic Stability*. Clarendon Press, Oxford, 1961.

[5] Karmakar, P. K. and Das, P. Instability analysis of cosmic viscoelastic gyro-gravitating clouds in the presence of dark matter. *Astrophysics and Space Science,* 362: 142. 1-13, 2017.

[6] Das, P. and Karmakar, P. K. Instability behaviour of cosmic gravito-coupled correlative complex bi-fluidic admixture. *Europhysics Letters*, 120: 19001. p1-p7, 2017.

[7] Tsiklauri, D. Jeans instability of interstellar gas clouds in the background of weakly interacting massive particles. *Astrophysical Journal,* 507: 226-228, 1998.

[8] Karmakar, P. K. and Das, P. Stability of gravito-coupled complex gyratory astrofluids. *Astrophysics and Space Science,* 362: 115. 1-9, 2017.

[9] Janaki, M. S., Chakrabarti, N., and Banerjee, D. Jeans instability in a viscoelastic fluid. *Physics of Plasmas,* 18: 012901. 1-5, 2011.

[10] Gresho, P. M. and Sani, R. L. *Incompressible Flow and the Finite Element Method.* Wiley, New York, 1998.

[11] Frenkel, J. *Kinetic Theory of Liquids.* Oxford University Press, Oxford, 1946.

[12] Brevik, I. Temperature variation in the dark cosmic fluid in the late universe. *Modern Physics Letters A,* 31: 1650050. 1-12, 2016.

[13] Raymond, J. and Skarda, L. Convective Instability of a Gravity Modulated Fluid Layer With Surface Tension Variation. AIAA-98-2599, New Mexico, 1998.

[14] Borah, B., Haloi, A., and Karmakar, P. K. A generalized hydrodynamic model for acoustic mode stability in viscoelastic plasma fluid. *Astrophysics and Space Science,* 361: 165. 1-11, 2016.

[15] Das, P. and Karmakar, P. K. Nonlinear waves in viscoelastic magnetized complex astroplasmas with polarized dust-charge variations. *AIP Advances,* 8: 015010. 1-14, 2018.

[16] Karmakar, P. K. and Dutta, P. Nonlinear eigen-structures in star-forming gyratory nonthermal complex molecular clouds. *Physics of Plasmas,* 25: 012306. 1-9, 2018.

[17] Ablowitz, M. J. *Nonlinear Dispersive Waves: Asymptotic Analysis and Solitons.* Cambridge University Press, New York, 2011.

[18] Wazwaz, A.-M. *Partial Differential Equations and Solitary Waves Theory.* Springer, Berlin, 2009.

[19] Tielens, A. G. G. M. *The Physics and Chemistry of the Interstellar Medium.* Cambridge University Press, Cambridge, 2005.

[20] Chandrasekhar, S. *An Introduction to the Study of Stellar Structure*. University of Chicago Press, Chicago, 1938.

[21] Camenzind, M. *Compact Objects in Astrophysics.* Springer, Berlin, 2007.

[22] Mihalas, D. and Mihalas, B. W. *Foundations of Radiation Hydrodynamics.* Oxford University Press, New York, 1984.

[23] Schwalbe, L. and Grilly, E. Thermal expansion of liquid normal hydrogen between 18.8 and 22.2 K. *Journal of Research of the National Bureau of Standards,* 89: 317-323, 1984.

[24] Adams, F. C. and Fatuzzo, M. Nonlinear waves and solitons in molecular clouds. *Astrophysical Journal,* 403: 142-157, 1993.

[25] Karmakar, P. K. and Haloi, A. Pulsational instability of complex charge-fluctuating magnetized turbulent astroclouds. *Astrophysics and Space Science,* 362: 152. 1-9, 2017.

[26] Dovner, P. O., Eriksson, A. I., Boström, R., and Holback, B. Freja multiprobe observations of electrostatic solitary structures. *Geophysical Research Letters,* 21: 1827-1830, 1994.

[27] Eriksson, A. I., Holback, B., Dovner, P. O., Boström, R., Holmgren, G., André, M., Eliasson, L., and Kintner, P. M, Freja observatons of correlated small-scale density depletions and enhanced lower hybrid waves. *Geophysical Research Letters,* 21: 1843-1846, 1994.

APPENDIX-3.A

Table 3.1: Key instability featuring factors

Serial No.	Featuring item	Perturbed density	Density gradient	Phase portrait	Inference
1	Equilibrium temperature (T_o)	Solitary peaks shift inward, with no change in amplitude (figure 3.1(a))	Peaks shift inward, with field fluctuation amplitude increases, and vice-versa (figure 3.1(b))	Closed geometric structure, conservative in nature, fixed point unaffected with T_o (figure 3.1(c))	Destabilizer
2	Referral frame velocity (μ)	Solitary peaks shift outward, with amplitude getting reduced (figure 3.2(a))	Peak shifts outward, with field fluctuation amplitude decreases. (figure 3.2(b))	Closed geometric structures, conservative, Phase portrait contract (figure 3.2(c))	Stabilizer
3	Generalized effective viscosity (χ)	Solitary peaks shift outward, with no change in amplitude (figure 3.3(a))	Peak shifts outward, with field fluctuation amplitude decreases (figure 3.3(b))	Closed geometric structure, conservative in nature, fixed point unaffected with χ (figure 3.3(c))	Stabilizer
4	Relaxation time (τ_m)	Same as 1	Same as 1	Same as 1	Destabilizer
5	Number density (n_0)	Same as 1	Same as 1	Same as 1	Destabilizer
6	Polytropic index (n)	Same as 3	Same as 3	Same as 3	Stabilizer

7	Volumetric expansion coefficient (γ)	Similar to 1, peak-to-peak separation decreases	Similar to 1, amplitude drastically enhances	Same as 1	Destabilizer
8	Fluid complexity	Peak-spacing decreases with complications, but with same amplitude (figure 3.8(a))	Solitary field peak-separation decreases with complications with variable amplitude (figure 3.8(b))	Closed geometric structure, conservative in nature, fixed point unaffected (figure 3.8(c))	Destabilizer